Pergamon

*Atmospheric Environment* Vol. 28, No. 4, pp. 713–721, 1994
Elsevier Science Ltd

1352–2310/94 $6.00 + 0.00

# SINGLE-STATION INTEGRAL MEASURES OF ATMOSPHERIC STAGNATION, RECIRCULATION AND VENTILATION

K. JERRY ALLWINE and C. DAVID WHITEMAN
Pacific Northwest Laboratory, P.O. Box 999, Richland, Washington 99352, U.S.A.

(*First received* 9 *June* 1993 *and in final form* 1 *September* 1993)

**Abstract**—Mathematical definitions of integral quantities used to characterize the stagnation, recirculation and ventilation potential of various airsheds are proposed. These integral quantities can be calculated from wind data collected at fixed time intervals and at fixed heights in the atmosphere, and could be calculated, for example, from data from ground-based remote wind profilers. These integral quantities, since they are calculated from data at single stations, provide useful characterizations of the flow at individual measurement points, but are true measures of the transport of a plume only under idealized homogeneous wind conditions.

The utility of these single-station measures for characterizing the air pollution transport potential of an airshed is illustrated using three months of hourly surface and radar profiler measurements of horizontal wind speed and direction collected at three locations in the Colorado Plateaus Basin region of Arizona during the winter of 1990. A surface station at Bullfrog Basin, located on a sheltered basin floor and exposed to diurnal wind systems, experienced stagnations 62% of the time, recirculations 34% of the time, and ventilations 8% of the time. A surface station at Desert View, located on the south rim of the Grand Canyon and exposed to synoptic-scale wind systems, experienced stagnations 8% of the time, recirculations 4% of the time, and ventilations 35% of the time. A radar profiler station at Page, Arizona, experienced stagnations about 20% of the time and recirculations about 25% of the time during the winter at heights below ~400 m a.g.l.; above this height, to levels near 1100 m a.g.l. (the approximate height of surrounding plateaus), the frequency of stagnations and recirculations dropped rapidly, and the frequency of ventilations ranged from 40 to 70%.

*Key word index*: Air pollution transport, complex terrain meteorology, airshed carrying capacity, plume trajectories.

## 1. INTRODUCTION

Stagnation, recirculation and ventilation are terms that indicate special types of flow conditions that have important consequences for the dispersion of air pollutants. Stagnations are events where atmospheric flows decrease in speed, or stop altogether, allowing pollutants to build up in stagnant air in the vicinity of the pollutant sources. Recirculations are events in which polluted air is initially carried away from the source but later returns to produce a high pollution episode. Ventilations, on the other hand, are events in which polluted air is replaced or diluted by fresh air. Ventilation can occur by fresh air sweeping in to replace polluted air, or by polluted air being diluted by turbulent mixing with clean air, such as during times of convective boundary layer growth. The method described in this paper addresses ventilation occurring only by fresh air sweeping in to replace polluted air (horizontal advection). This limit on the definition of ventilation is a result of the analysis method using horizontal winds as the only input.

In air pollution work, the three terms are often used in a general sense, but are rarely defined mathematically to quantify the flow character. In this paper we develop mathematical definitions of these terms by focusing directly on the relevant atmospheric transport conditions, irrespective of pollution levels. Integral quantities representative of stagnation, recirculation and ventilation are defined, and calculations of these quantities from single-station measurements are illustrated using three months of hourly wind data from two surface stations and from a radar wind profiler in the Grand Canyon region of Arizona.

## 2. METHODOLOGY

Consider a time series of $N$ discrete data point pairs ($D_i$, $U_i$) of measured meteorological wind directions, $D_i$ (direction from which the wind is blowing; clockwise from north) and wind speeds, $U_i$, for $i = 1, 2, \ldots, N$. These data can be expressed as horizontal wind vectors $\vec{V}_i$, (direction toward which the wind is blowing) where the series of vectors is resolved into north–south (positive toward north) and east–west (positive toward east) components, respectively, as follows:

$$n_i = U_i \cos(D_i - 180) \quad (1)$$

$$e_i = U_i \sin(D_i - 180). \quad (2)$$

This results in a discrete time series of horizontal wind vectors (notation illustrated in Fig. 1) where the magnitude of

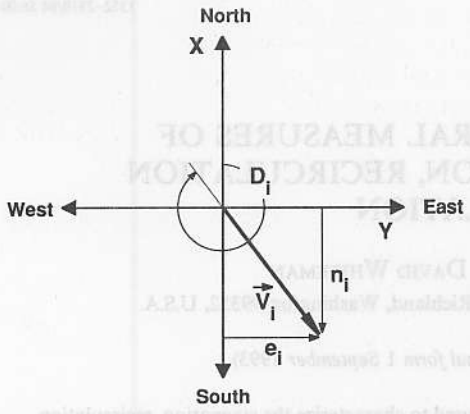


Fig. 1. Definition of coordinate system and notation used in equations to resolve the meteorological wind vector into components.

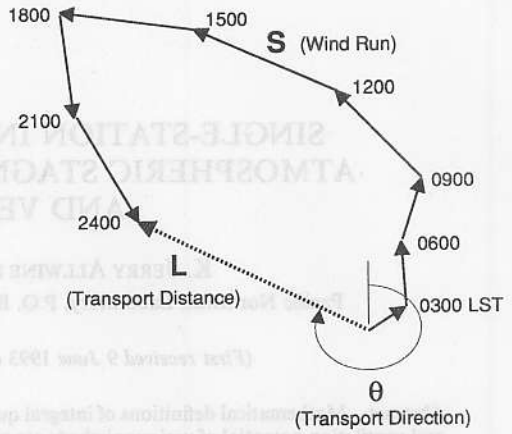


Fig. 2. Illustration of the definitions of wind run $S$, transport distance $L$ and transport direction $\theta$ assuming a 24-h transport time and 3-h-average observations.

each vector is:

$$|\vec{V}_i| = U_i = \sqrt{n_i^2 + e_i^2}. \quad (3)$$

The time, $t_i$, of each data point is

$$t_i = t_0 + (i-1)T \quad (4)$$

where $t_0$ is the time of the first data point and $T$ is the averaging interval of the data. The individual vectors in the time series may represent, for example, a series of hour-average wind vectors from a surface wind station, or half-hourly observations from each range gate of a vertically pointing remote sensing device such as a Doppler sodar or radar profiler.

We then define a set of discrete integral quantities that are computed at each time $t_i$, as follows:

$$S_i = T\sum_{j=i}^{i+p} |\vec{V}_j| \quad \text{wind run} \quad (5)$$

$$X_i = T\sum_{j=i}^{i+p} n_j \quad \text{north–south transport distance} \quad (6)$$

$$Y_i = T\sum_{j=i}^{i+p} e_j \quad \text{east–west transport distance} \quad (7)$$

$$L_i = \sqrt{X_i^2 + Y_i^2} \quad \text{resultant transport distance} \quad (8)$$

$$\theta_i = \arccos\left(\frac{X_i}{L_i}\right), \quad Y_i \geq 0$$

$$\theta_i = 360 - \arccos\left(\frac{X_i}{L_i}\right), \quad Y_i < 0 \quad \text{transport direction} \quad (9)$$

$$R_i = 1 - \frac{L_i}{S_i}, \quad (0 \leqslant R \leqslant 1) \quad \text{recirculation factor} \quad (10)$$

where

$i = 1, \ldots, N-p$

$p = \tau/T - 1, \quad 0 \leqslant p < N, [T \leqslant \tau < NT]$

and $\tau$ is the desired transport time. The resultant transport direction is measured clockwise from north and represents the direction toward which a parcel will travel. Figure 2 illustrates the calculation of the integral quantities determined from equations (5), (8) and (9).

Equations (5)–(10) give a "running" determination of the integral transport quantities. That is, at every observation time, $t_i$, the integral transport quantities are calculated, with time $t_i$ representing the transport start time and time $t_i + \tau$ representing the transport end time. The resultant transport distance and direction define the ending location of a parcel at time $t_i + \tau$ that "left" the sensor location at time $t_i$. The quantity $S_i$ is a measure of the total distance that the parcel traveled from time $t_i$ to time $t_i + \tau$. These quantities would be a correct measure of transport in an ideal homogeneous wind field. However, a homogeneous wind field is not normally experienced in real situations, especially in complex terrain. Consequently, these integral measures of transport are not true measures of the transport of a plume, but rather should be considered as characteristics of the flow at the measurement point. The intent is that these single-station quantities will prove useful for characterizing air pollution transport characteristics of various airsheds and regions.

The wind run $S$ divided by the transport time $\tau$ is the scalar average wind speed, $L$ divided by $\tau$ is the vector average wind speed, and $\theta - 180°$ is the vector average meteorological wind direction (direction from which the wind blows, clockwise from north). The recirculation factor $R$ gives an indication of the presence of local recirculations on time scales comparable with $\tau$. When $R$ is equal to 0, straight-line transport has occurred with no recirculation; when $R$ is equal to 1, zero net transport has occurred over the time interval $\tau$, and there has been a complete recirculation where the air parcel has returned to its origin. The wind run is used as a measure of stagnation; a value of $S$ equal to 0 is the theoretical value defining total stagnation, that is, no winds and thus no transport. Ventilation is characterized by low values of $R$ and high values of $S$.

It should be noted that equation (10) has a mathematical singularity (divide by zero) for $S$ equal to 0. However, $L$ is also equal to 0 when $S$ is equal to 0. Consequently, in the mathematical limit, $R$ is defined when $S$ is equal to 0, and has a value of 0, implying no recirculation. It should also be noted that for any site the sum of the percent occurrence of stagnation, recirculation and ventilation does not necessarily total 100% because all possible flow conditions are not covered with these definitions. Also, the sum of the three can total to more than 100% at some locations, because stagnation events and recirculation events can occur simultaneously.

## 3. APPLICATION

The defining equations and methodology in the previous section can be applied to any time series of

wind vectors at a single station. The methodology could be used at individual sites to determine if transport characteristics at the site exceed certain critical values for stagnation, recirculation or ventilation. The critical values would be determined on the basis of investigations in many regions. Alternatively, the methodology could be used to compare sites within a region to identify air pollution dispersion regimes, or could be applied to data from ground-based remote wind sensors (e.g. Doppler sodars or radar profilers) to determine the change of transport characteristics with height.

One approach for classifying locations according to stagnation, recirculation and ventilation potential is to compare the average (over the entire period-of-record) daily ($\tau = 24$ h) wind run $\bar{S}$ and average recirculation factor $\bar{R}$ with predetermined critical transport indices (CTIs), such as:

$\bar{S} \leqslant \bar{S}_c \Rightarrow$ Site Prone to Stagnation

$\bar{R} \geqslant \bar{R}_c \Rightarrow$ Site Prone to Recirculation

$\bar{R} \geqslant \bar{R}_{cv}$ and $\bar{S} \geqslant \bar{S}_{cv} \Rightarrow$ Site Prone to Ventilation

where $\bar{S}_c$ and $\bar{R}_c$ are the average daily CTIs for stagnation and recirculation, respectively, and $\bar{S}_{cv}$ and $\bar{R}_{cv}$ are the average daily CTIs for ventilation.

A second approach for classifying stagnation, recirculation and ventilation potential is to compare individual daily ($\tau = 24$ h) values of $S$ and $R$ with predetermined daily CTIs, $S_c$, $R_c$, $S_{cv}$ and $R_{cv}$, and to express the result in terms of the percentage of the time that the limits are exceeded during the period-of-record.

In the following section we illustrate the utility of the integral quantities by performing calculations for three locations in the Colorado Plateaus Basin region (Fig. 3) using data from the Navajo Generating Station Winter Visibility Study of January–March 1990 (Richards *et al.*, 1991). As part of this study, a network of towers and remote sensing wind profilers was installed in the Grand Canyon region to determine the regional evolution of three-dimensional wind structure. The region was known from previous work to be influenced by deep wintertime inversions and to undergo lengthy periods of stagnation and recirculation (e.g. Whiteman, 1992).

Because diurnal thermally driven flows (mountain–valley winds, slope winds, and land–lake breezes) are frequently encountered in the Grand Canyon region, we have chosen $\tau = 24$ h for most calculations. We first demonstrate the methodology using data from two surface stations. This is followed

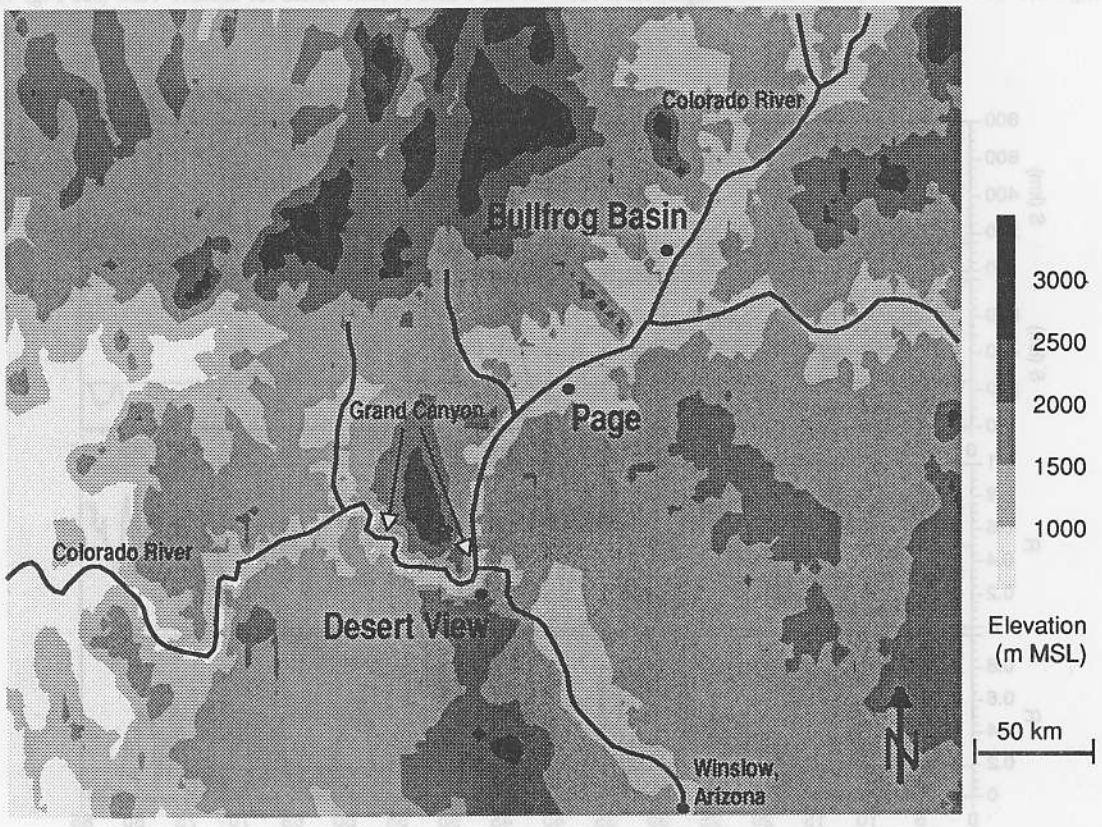


Fig. 3. Locations of two surface observation stations (Bullfrog Basin and Desert View) and the radar profiler (Page) in the Grand Canyon region.

by calculations using data from a wind profiler and, finally, the effects of different transport times ($1 \leqslant \tau \leqslant 48$ h) are investigated by extending our analysis of the data from the two surface stations.

### 3.1. *Surface observations*

The surface data to be analysed consist of hour-average wind observations collected by Sonoma Technology, Inc., at 10 m a.g.l. on towers located at Bullfrog Basin (1130 m m.s.l.) and Desert View (2283 m m.s.l.) in the Colorado Plateaus Basin region (Fig. 3). The Bullfrog Basin site is on a sheltered basin floor where diurnal forcing of the winds is frequently observed. The Desert View site is on the South Rim of the Grand Canyon and is well exposed to synoptic wind influences. The period of record is the 86-day period from 1 January (Julian day 1) to 27 March 1990 (Julian day 86).

Figure 4 presents the hourly trace of the wind run and the recirculation factor for Bullfrog Basin and Desert View for $\tau = 24$ h. The average daily ($\tau = 24$ h) wind run over the 86-day period, $\bar{S}$, for Bullfrog Basin is 145 km compared to 250 km for Desert View. These represent average daily wind speeds of 1.7 and 2.9 m s$^{-1}$, respectively. The average daily recirculation factor, $\bar{R}$, for Bullfrog Basin is 0.49 and for Desert View is 0.18.

For purposes of illustration, we may classify the stagnation, recirculation, and ventilation potential for individual stations within a region by setting average daily CTIs. For example, for the Grand Canyon region we may propose $\bar{S}_c = 170$ km ($\sim 2$ m s$^{-1}$ average daily wind speed), $\bar{R}_c = 0.4$, $\bar{S}_{cv} = 250$ km ($\sim 3$ m s$^{-1}$ average daily wind speed), and $\bar{R}_{cv} = 0.2$. Applying these CTIs to Bullfrog Basin and Desert View gives the result that Bullfrog Basin is prone to stagnations and recirculations, and Desert View is prone to ventilations. Of course, these results are expected because the preliminary CTIs were chosen based on the *a priori* knowledge that Bullfrog Basin experiences frequent stagnations and recirculations, and that Desert View is well exposed to synoptic-scale circulation systems.

To illustrate the computations of the percent occurrence of stagnation, recirculation, and ventilation events at individual stations we may, for example, set daily CTIs for the Grand Canyon region to be: $S_c = 130$ km (daily average wind speed of $\sim 1.5$ m s$^{-1}$), $R_c = 0.6$, $S_{cv} = 250$ km (daily average wind speed of $\sim 3$ m s$^{-1}$), and $R_{cv} = 0.2$, respectively. Then, for example, from analysis of the time series of $S$ for Bullfrog Basin (see Fig. 4), $S$ values less than 130 km occurred 62% of the time, indicating that stagnation events occurred 62% of the time at Bullfrog Basin. Additional analysis of the time series of $S$ and $R$ for Bullfrog Basin gives recirculation and ventilation events occurring 34 and 8% of the time, respectively. Analysis of the $S$ and $R$ time series for Desert View (see Fig. 4)

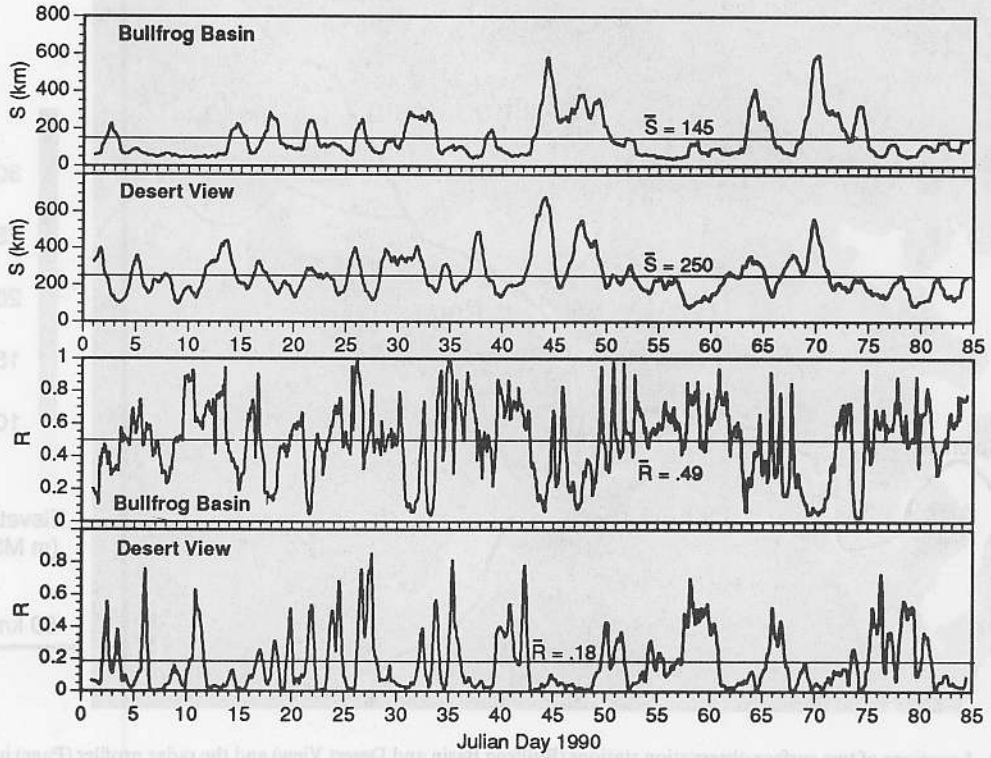


Fig. 4. Daily ($\tau = 24$ h) wind runs and recirculation factors for Bullfrog Basin and Desert View.

results in stagnation, recirculation and ventilation events occurring 8, 4, and 35% of the time, respectively.

Figure 5 gives a complete visual representation of the stagnation, recirculation and ventilation character of the Bullfrog Basin and Desert View sites. This figure is not necessary (albeit it is sufficient) for determining the percent occurrences of stagnation, recirculation and ventilation events for a site. Rather, it is given here to more fully illustrate the differences between the Bullfrog Basin and Desert View sites, and to reveal the sensitivity of the percent occurrences of stagnations, recirculations and ventilations to the choice of the CTIs.

The top panel in Fig. 5 gives the percent occurrence of stagnation (values on top axis), recirculation (values on left axis) and ventilation (values of isopleths) at Bullfrog Basin as a function of critical values of $S$ (values on bottom axis) and $R$ (values on right axis), and the bottom panel gives the percent occurrences for Desert View. The percent occurrence of stagnation, recirculation and ventilation events can be read directly from the figure given the CTIs identified above. For example, the intersection of $R_{cv}$ and $S_{cv}$ for Bullfrog Basin occurs at an isopleth value of 8%, which is the percent occurrence of ventilation at Bullfrog Basin. The percent occurrence of recirculations is determined as the value on the left axis intersected by $R_c$ extended left from the right axis. Bullfrog Basin shows 34% recirculation for $R_c$ of 0.6. The percent occurrence of stagnations is determined as the value on the top axis intersected by $S_c$ extended up from the bottom axis. For example, Bullfrog Basin shows 62% stagnation for $S_c$ of 130 km.

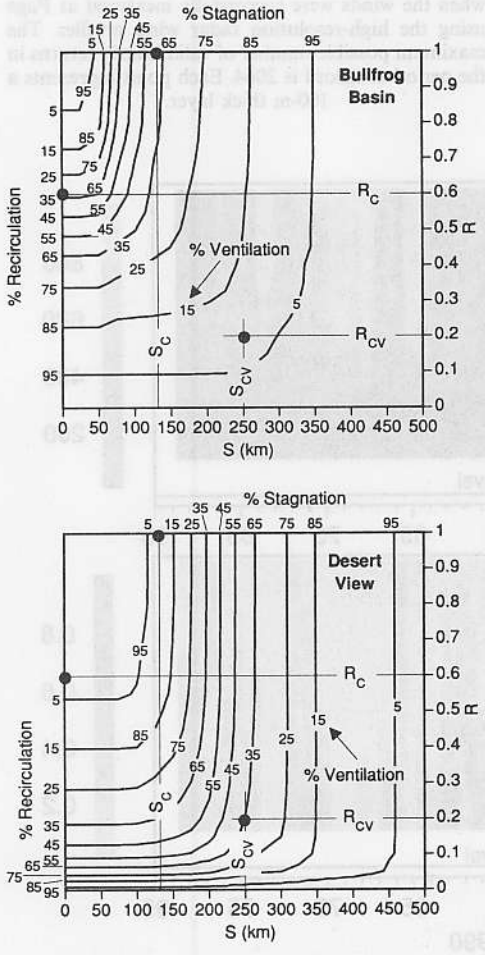


Fig. 5. Plots of percent occurrence of stagnations, recirculations and ventilations for Bullfrog Basin and Desert View.

Each panel in Fig. 5 was developed from an isopleth plot of the joint ($S$–$R$) cumulative percent occurrence calculated for each site. The joint ($S$–$R$) cumulative percent is required because the percent occurrence of ventilation is determined from both $R$ and $S$, whereas the percent occurrence of recirculation is determined from $R$ only and the percent occurrence of stagnation is determined from $S$ only. Once the joint cumulative percentages are determined, the individual $R$ and $S$ cumulative percentages are also available.

The joint ($S$–$R$) cumulative percent occurrence for each site was calculated by first binning every ($S$, $R$) pair of values for each time step into bins of $S$ progressing from 700 to 0 km in steps of 25 km (28 bins), and bins of $R$ progressing from 0 to 1 in steps of 0.05 (20 bins). The total number of data points in the 28-by-20 array of bins is the total number of time steps (2064 for hourly data for 86 days). Next, the joint percent occurrence for each bin of the array was calculated as the number of points in each bin divided by the total number of data points times 100. Finally, the joint cumulative percent for each bin was determined as the sum of the joint percents from all bins proceeding from $S$ equal to 700 to the bin of interest, and proceeding from $R$ equal to 0 to the bin of interest. For example, the joint cumulative percent of the bin containing $S$ equal to 0 and $R$ equal to 1 is 100%.

The values of the isopleths in each panel of Fig. 5 give, therefore, not only the percent occurrence of ventilation, as labeled in the figure, but also identify the joint ($S$–$R$) cumulative percent occurrence for the particular site. The percent recirculation values on the left axis are determined as 100% minus the values of the isopleths where the isopleths intersect the left axis, and the percent stagnation values on the top axis are determined as 100% minus the values of the isopleths where the isopleths intersect the top axis.

The values of the CTIs used above are given solely to demonstrate the utility of the integral quantities and are not intended to be the definitive set of CTIs for the Grand Canyon region, or any region. A proper determination of these indices, however, will be very important for characterizing dispersion characteristics of various airsheds. The primary approach for setting these indices is to calculate the integral quantities for numerous stations in many airsheds of known dispersion potential. A general set of CTIs can then be determined from these results.

### 3.2. *Radar profiler observations*

The Page, Arizona, wind profiler site is located in the Colorado Plateaus Basin (Fig. 3) on a hill overlooking Lake Powell. Radar profiler data from this station extend from the floor of the basin to elevations above the ridgetops of the surrounding mountains. The data set analysed consists of hour-average wind data from the radar wind profiler (UHF radar system) operated by NOAA's Wave Propagation Laboratory. The period of record analysed is the 86-day period from 8 January (Julian day 8) to 3 April 1990 (Julian day 93). Horizontal winds were measured through 20 100-m-thick layers, with the midpoint elevation of the first layer at 1470 m m.s.l. (150 m a.g.l.) and the midpoint elevation of the top layer at 3397 m m.s.l. (2077 m a.g.l.).

Radar wind profilers depend on turbulence-produced refractive index fluctuations of both temperature and humidity and their cross-correlations for determining winds from Doppler-shifted frequencies (Neff, 1990). Since radars depend on the presence of turbulence for the scattering of the radio waves, they can suffer from a lack of valid signal returns (signal strength comparable to noise level) from the portions of the atmosphere where turbulence is weak. Figure 6 shows that the number of valid returns decreases with height at Page. In the following analyses only the 11 lowermost layers, which had 25% or greater sample recovery, are utilized. The midpoint elevation of the first layer is 1470 m m.s.l. and the midpoint elevation of the eleventh layer is 2484 m m.s.l.

Plots of the daily ($\tau = 24$ h) wind run and the daily recirculation factor for Page are given in Fig. 7. These

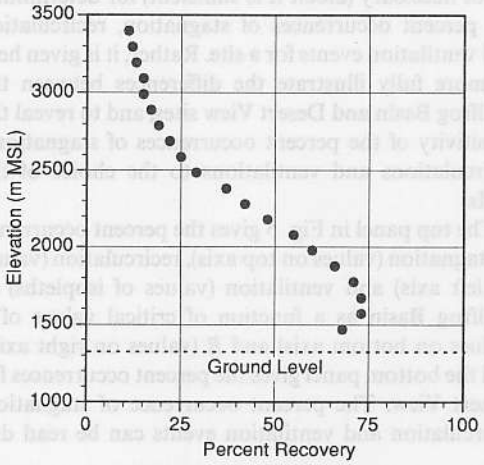


Fig. 6. Percentage of total hours in the study period when the winds were successfully measured at Page using the high-resolution radar wind profiler. The maximum possible number of valid hourly returns in the period of record is 2064. Each point represents a 100-m thick layer.

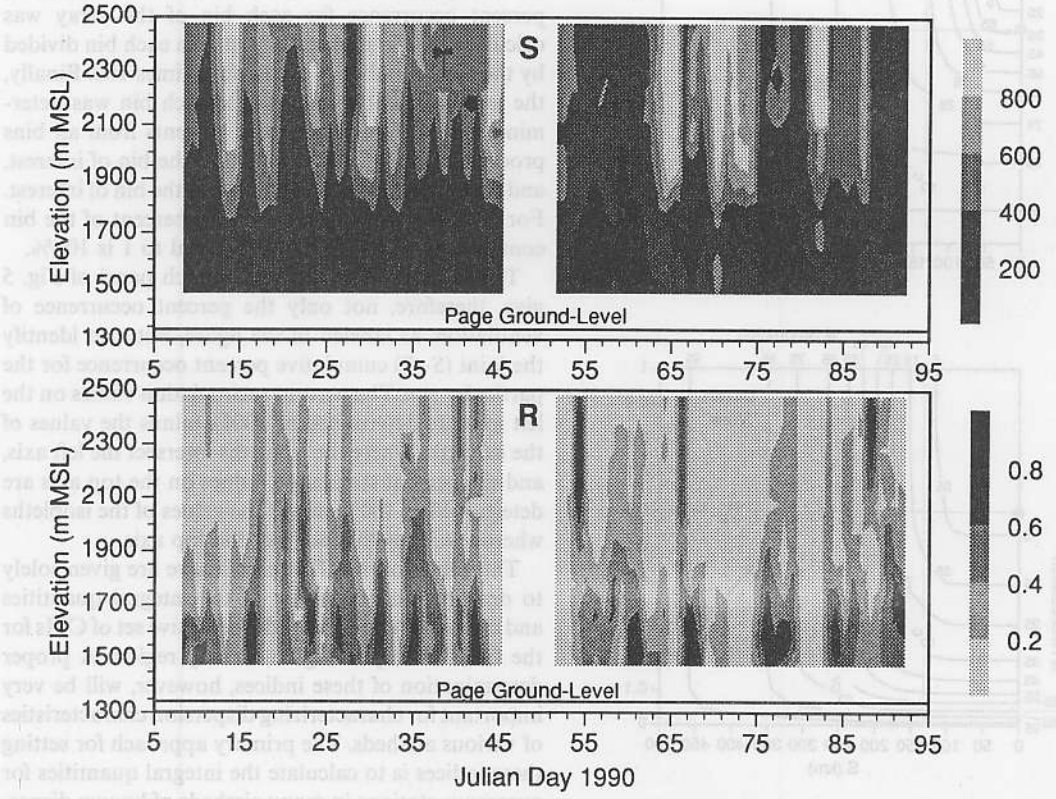


Fig. 7. Time–height cross-sections of daily ($\tau = 24$ h) wind run $S$ (km), and daily recirculation factor $R$ at Page, Arizona.

transport quantities are plotted as a function of height for the 86-day period of record. It should be noted that a 6-day period (Julian days 46–51) of data is missing and is indicated by the white areas in the figure. Also a few values in each plot in Fig. 7 were not calculated because less than 5 hourly observations were available at a given height for that day. In these cases, the transport quantities were estimated by linear interpolation from the surrounding calculated values or by using the nearest calculated value. When more than 5 hourly wind observations were available at a height for any 24-h period, the daily transport quantities were calculated at that height by first linearly interpolating from the valid observations to estimate the missing hourly observations.

Daily recirculation factors greater than 0.6 were encountered at Page during 20% of the study period at elevations less than about 1700 m m.s.l. (Fig. 7). Above 1900 m m.s.l. (to $\sim$2500 m m.s.l., top of the analysis), the majority of days exhibited $R$ values less than 0.2. Some days, however, had recirculation values greater than 0.4 at elevations above 1900 m m.s.l., and in two cases (days 54 and 88), strong recirculations ($R \geqslant 0.8$) were observed at roughly 2200–2400 m m.s.l. ($\sim$900–1100 m a.g.l.). Considering recirculation defined as previously, $R \geqslant 0.6$, then the Page area experiences recirculations about 20% of the time during winter at elevations below $\sim$1700 m m.s.l. Stagnation was evident about 25% of the time below $\sim$1700 m m.s.l., based on the previous definition of stagnation, $S \leqslant 130$ km.

On some days the recirculation factor was less than 0.2 through the full profile. Such cases typically occur following the breakup of the basin temperature inversion by passing synoptic-scale disturbances. In these cases strong winds descend into the depths of the basin from above, and wind directions are often nearly invariant with height. Such was the case on day 18 when winds were from the northeast. Figure 7 shows the daily wind run to be from 400 km to greater than 600 km through much of the profile. This translates to average wind speeds from $\sim$4.6 m s$^{-1}$ to greater than $\sim$6.9 m s$^{-1}$ through much of the profile. Considering our previous definition of ventilation ($R \leqslant 0.2$, $S \geqslant 250$ km), then from Fig. 7, ventilation below $\sim$1700 m m.s.l. is experienced roughly 10% of the time during winter.

Days 54–64 exhibited recirculations and stagnations through a significant elevation range within the basin. Such periods are expected to have significant air pollution implications since pollution generated within the basin could remain confined within the basin for several days.

The daily ($\tau = 24$ h) recirculation factor averaged over the entire period-of-record, $\bar{R}$, at each elevation is given in Fig. 8. $\bar{R}$ at the upper levels of the Page profile is comparable with the value calculated for the Desert View location. The Desert View location is at the same elevation as the upper-level measurements at Page. The fact that the $\bar{R}$ values at the two locations are

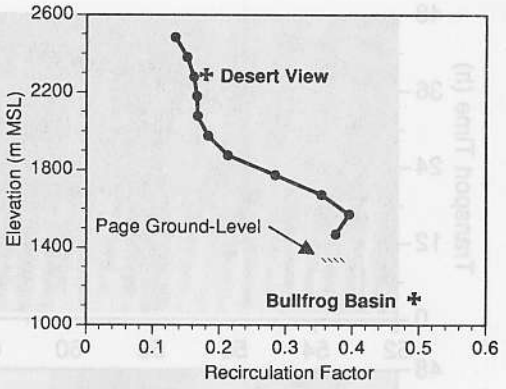


Fig. 8. Average daily ($\tau = 24$ h) recirculation factor as a function of height for the Page, Arizona, radar profiler. Recirculation factors for the Bullfrog Basin and Desert View towers are shown for comparison.

comparable supports the view that the Desert View site is well exposed to the synoptic winds. A reasonable correlation ($r^2 = 0.7$) in the wind direction observations at the two locations also supports this view. The average daily recirculation factor in the lowest portion of the Page profile (ignoring the lowest point) shows a tendency to approach the value of $\bar{R}$ measured in Bullfrog Basin, if the Page $R$ profile is extended to ground-level at Bullfrog Basin. The $\bar{R}$ profile defined by the Page radar profiler and the Bullfrog Basin tower is probably a reasonable representation of the $\bar{R}$ profile throughout this portion of the Colorado River Valley.

### 3.3. *Surface observations—variable* $\tau$

The tower observations at Bullfrog Basin and Desert View are analysed in more detail in this section by investigating the behavior of the recirculation factor over a range of transport times. The focus is on identifying the effect on $R$ of oscillations in the data at periods other than 24 h. Figure 9 shows $R$ as a function of $\tau$ at Bullfrog Basin and Desert View for a 20-day period. Several important features are apparent in this figure. In the top panel of Fig. 9, the "fingers" extending downward from an imaginary horizontal line at $\tau \approx 24$ h, and spaced at intervals of roughly 1/2 day, are indicative of the dominant 24-h period in the Bullfrog Basin data. The behavior of $R$ as a function of $\tau$ for Desert View is indicative of dominant oscillations in the data at periods of several days. Shorter period oscillations (order of 24 h) are also indicated in the Desert View data between days 57 and 61. Theoretically, an oscillation of period $P$ will result in $R = 1$ at all times for $\tau = P$. "Fingers", with a value 1 at their centers, would extend downward from $\tau = P$ and be spaced in time at intervals of $P/2$.

Figure 10 gives the average $R$ over the entire 86-day period as a function of transport time for Bullfrog Basin and Desert View. The Bullfrog Basin curve rises more steeply than the Desert View curve for $\tau$ less than 24 h because of the dominant 24-h oscillation in the

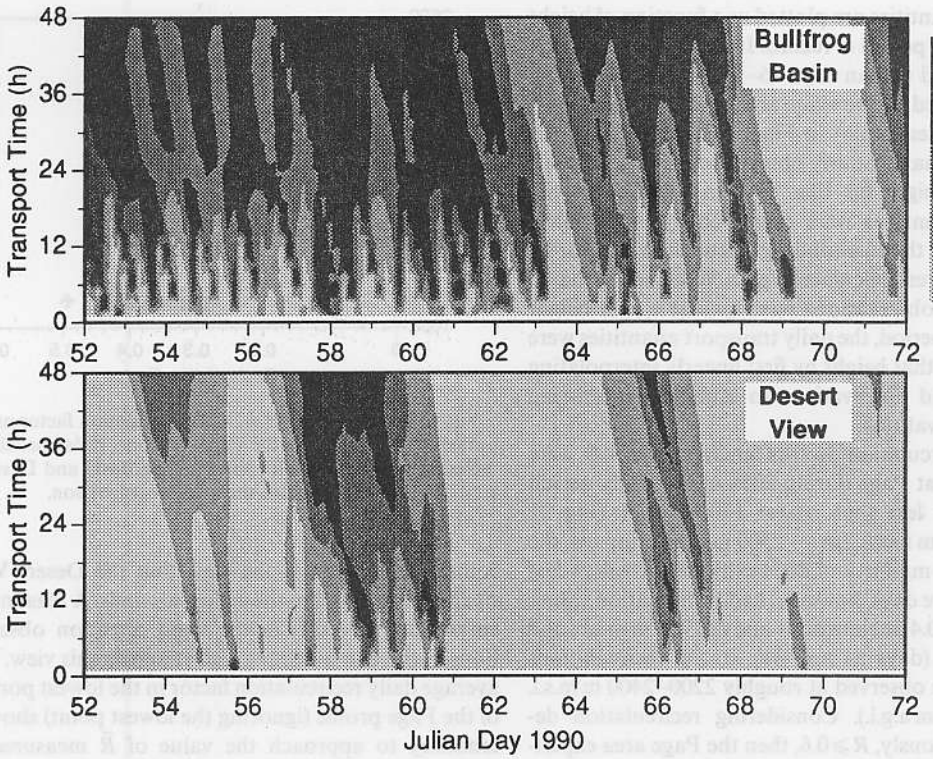


Fig. 9. Recirculation factor as a function of transport time for a 20-day period at Bullfrog Basin and Desert View.

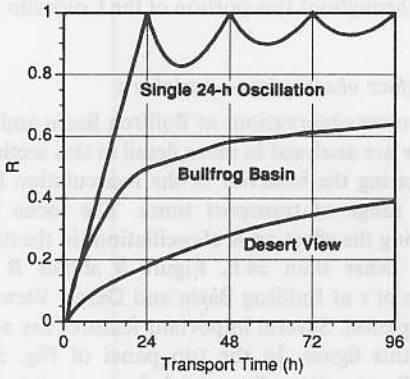


Fig. 10. Average recirculation factor as a function of transport time at Bullfrog Basin and Desert View.

winds at Bullfrog Basin. The curves for both locations approach the same flatter slope after roughly $\tau = 48$ h because of the influence on $R$ of the synoptic-scale oscillations (periods of several days) observed at both locations.

For reference, a third curve in Fig. 10 shows the values of average $R$ calculated from a pure sinusoidal wind oscillation of period $P = 24$ h. The ideal wind oscillation is assumed to be zero in the north–south direction and to vary sinusoidally with an amplitude of 1 m s$^{-1}$ in the east–west direction. $R$ is exactly equal to 1 at all $\tau$ that are multiples of $P$. In addition, the local minima apparent in this ideal curve are described as

$$R_n = 1 - \frac{1}{2(2n+1)}; \qquad n = 1, 2, 3, \ldots \tag{11}$$

at the corresponding discrete transport times of $\tau_n = (2n+1)P/2$. Close inspection of the Bullfrog Basin curve in Fig. 10 shows that the curve dips in between $\tau$ values that are multiples of 24 h, another indicator that the Bullfrog Basin site experiences frequent diurnal wind oscillations.

## 4. SUMMARY AND CONCLUSIONS

Single-station integral measures of stagnation, recirculation and ventilation are defined to provide a means of quantifying the air pollution transport potential of various airsheds and regions. These measures can be applied to wind data collected at fixed time intervals and at fixed heights in the atmosphere, and are suitable for use with data from ground-based remote wind profiling sensors. These single-station integral measures are not true measures of the transport of a plume, but rather should be considered as characteristics of the flow at the measurement point.

The integral quantities should be computed over a range of transport times to identify the dominant time-

scales of motion responsible for recirculation. In complex terrain, the dominant period of oscillation of the winds is often 24 h because of the potential for frequently encountered diurnal thermally driven flows (mountain–valley winds, slope winds, and land–lake breezes). Since this paper deals with a data set from a complex terrain area, the focus of our analyses is on 24-h transport times.

Application of the single-station measures of stagnation, recirculation and ventilation is illustrated using three months of wintertime hourly wind data from two 10-m towers (at Bullfrog Basin and Desert View) and one radar wind profiler (at Page) located in the Grand Canyon region of the Colorado Plateaus Basin. For purposes of illustration, daily critical transport indices (CTIs) were defined to be $S_c = 130$ km, $R_c = 0.6$, $S_{cv} = 250$ km, and $R_{cv} = 0.2$. Using these CTIs and the test conditions

$S \leqslant S_c \Rightarrow$ Stagnation

$R \geqslant R_c \Rightarrow$ Recirculation

$R \leqslant R_{cv}$ and $S \geqslant S_{cv} \Rightarrow$ Ventilation

we determined the frequencies of stagnation, recirculation, and ventilation over the period-of-record for Bullfrog Basin (62, 34, and 8%, respectively) and for Desert View (8, 4, and 35%, respectively). These results are consistent with the exposures of the stations; the Bullfrog Basin site is on a sheltered basin floor where diurnal forcing of the winds is frequently observed, and the Desert View site is on the South Rim of the Grand Canyon and is well exposed to synoptic wind influences. The analysis of the radar profiler data indicated that the Page area has frequent stagnations ($\sim$20% of the time) and recirculations ($\sim$25% of the time) during the winter at heights below $\sim$400 m a.g.l. Above this height, to levels of $\sim$1100 m a.g.l. (the approximate height of surrounding plateaus), the frequency of stagnations and recirculations dropped rapidly, and the frequency of ventilations ranged from 40 to 70%. In general, the daily integral transport characteristics at Page reveal many periods of recirculation and stagnation at various heights throughout the study period, especially below $\sim$600 m a.g.l.

A vertical profile of the daily ($\tau = 24$ h) recirculation factor averaged over the entire period-of-record was calculated from the radar profiler data and compared with average $R$ values from the two surface stations. The Desert View average $R$ value (0.18) was approximately equal to the Page $R$ value (0.16) at the same elevation. The Bullfrog Basin $R$ value (0.49; $\sim$300 m below the lowest Page measurement height) is larger than the $R$ value (0.40) at the lower heights at Page. Combining the results from Page and Bullfrog Basin gives an average $R$ profile that is probably representative of the Colorado Plateaus Basin upstream from the Grand Canyon. This profile quantifies the recirculation potential of this portion of the Colorado Plateaus Basin airshed during winter.

The utility of this method of quantifying stagnations, recirculations, and ventilations would be improved by a comprehensive investigation of these transport quantities for climatically diverse locations and the development of a physical or statistical basis for determining the values of the critical transport indices (CTIs). These are topics for future investigation.

*Acknowledgements*—Data were provided by Arizona's Salt River Project. Analyses were funded by the U.S. Department of Energy (DOE) under Contract DE-AC06-76RLO 1830 as part of DOE's Atmospheric Studies in Complex Terrain (ASCOT) program and by Arizona's Salt River Project. The Pacific Northwest Laboratory is operated for DOE by Battelle Memorial Institute.

## REFERENCES

Neff W. D. (1990) Remote sensing of atmospheric processes over complex terrain. In *Atmospheric Processes over Complex Terrain* (edited by Blumen W.), Chapter 8. Meteorological Monographs, 23 (45), pp. 173–228. Am. Met. Soc., Boston.

Richards L. W., Blanchard C. L. and Blumenthal D. L. (1991) The Navajo generating station visibility study final report. Draft No. 2. Report STI-90200-1124-FRD2 to Salt River Project from Sonoma Technology, Inc., Santa Rosa, California, 16 April, 1991. Copies available from Prem Bhardwaja, Salt River Project, P.O. Box 52025, Phoenix, AZ 85072, U.S.A.

Whiteman C. D. (1992) Wintertime meteorology of the Grand Canyon region. Preprints of Sixth Conf. on Mountain Meteorology, Portland, Oregon, pp. 144–150. Am. Met. Soc., Boston.